First principles insights into Cs$_2$XAgCl$_6$ (X= Sc, Y) compounds for energy harvesting applications

S. A. Aldaghfag[a], Nasarullah[b], A. Aziz[b], M. Ishfaq[b], M. Yaseen[b,*], Hafsa[b],
S. Jamshaid[b]
[a]*Department of Physics, College of Sciences, Princess Nourah bint Abdulrahman
University, P. O. Box 84428, Riyadh 11671, Saudi Arabia*
[b]*Spin-Optoelectronics and Ferro-Thermoelectric (SOFT) Materials and Devices
Laboratory, Department of Physics, University of Agriculture Faisalabad,
Faisalabad 38040, Pakistan*

Herein, the investigation is presented to analyze the structural, electronic, optical, and thermoelectric features of Cs$_2$XAgCl$_6$ (X= Sc, Y) by applying the first principles approach. The confirmation of the stable structure of both compounds is reinforced by the negative values of formation enthalpies. The electronic band gaps (E$_g$) of 3.78/4.86 eV are computed for Cs$_2$ScAgCl$_6$ /Cs$_2$YAgCl$_6$ through Tran-Blaha modified Becke-Johnson (TB-mBJ) potential, correspondingly. The tolerance factor(τ) is found as 0.9 for Cs$_2$ScAgCl$_6$ and 1.0 for Cs$_2$YAgCl$_6$ which confirmed the stable cubic nature of both compounds. Optical factors like dielectric-function $\varepsilon(\omega)$, absorption coefficient $\alpha(\omega)$, and others related parameters are analyzed within 0 to 10 eV of energy span. Both compounds demonstrated high absorption in the ultraviolet region, rendering them as well-suited materials for photovoltaic applications. The calculated values of refractive index for Cs$_2$ScAgCl$_6$ and Cs$_2$YAgCl$_6$ indicated super-luminescent characteristics in the ultraviolet region. For thermoelectric (TE) features, electrical conductivity (σ/τ), figure of merit (ZT), power factor (PF), thermal conductivity (k/τ), and Seebeck coefficient (S) are calculated using the BoltzTraP code. According to the findings, both materials are advocated as promising candidates for thermoelectric and optoelectronic applications.

1. Introduction

The energy crisis is increasing day by day due to which fossil fuels and global warming have become the major problem of the world in the present era. To tackle such difficulties, improvements in energy conversion and creating storage technologies by halide double perovskites (HDPs) have attracted the researcher's attention massively. These advancements are surely not that easy to be implemented but luckily desired purposes have been accomplished by using HDPs [1]. HDPs consist of 90% of the elements of the periodic table with stable structures [2]. HDPs used in various applications including temperature sensors, superconductors, TE coolers, refrigerators, satellites, infra-red sensors, and memory storages devices [3].

HDPs are the class of quaternary halides symbolized by formula A$_2$BB′X$_6$. Where A-site positive ion and B are typically alkali or alkaline earth metals (not limited to), B´ is transition metal, rare earth element, or other trivalent metal ion and X is considered any halogen atom [4] [5]. Enamul Haque and his co-workers calculated the bandgap (E$_g$) of 3.15 eV for Cs$_2$BiAgCl$_6$ by using the ab-initio method and suggested it for applications in LEDs, transistors, X-ray detectors, and solar cells owing its satisfactory bandgap [6]. Li *et al.* prepared an ordinary stable (CH$_3$NH$_3$)$_2$AgSbI$_6$ halide which turned out to be a promising light absorber with an appropriate

---

optical E_g (1.93 eV) and got suggested as the best material for photovoltaic applications [7]. As for lead containing halide perovskites, despite of their extraordinary absorbent efficiency, the Pb toxicity and poor stability limit its mass production for commercialization that makes it essential to discover stable Pb-free materials [8] [9].

Recently, TE features of some double perovskites were investigated, and the outcomes predicted them highly efficient for energy harvesting applications. Amit Soni *et al.* reported first-principles calculations of the optoelectronic features of $Cs_2AgInCl_6$ for photovoltaic usage and computed direct bandgap (3.01 eV), confirming its superb absorption spectra in the visible energy range of 0 to 5 eV [10]. Noor *et al.* used DFT calculations for Cs_2ScInI_6 and Rb_2ScInI_6 to compute their optoelectronic and thermoelectric parameters. It was discovered that Cs_2ScInI_6/Rb_2ScInI_6 possess direct E_g of 0.95/0.90 eV, correspondingly, along with the ZT values of 0.75 for both compounds at room temperature [11]. Fatima Aslam *et al.* reported thermoelectric and optoelectronic features of $Cs_2InBiCl_6$, $Cs_2InBiBr_6$, and Cs_2InBiI_6 using DFT and found the bandgaps of 1.84 for $Cs_2InBiCl_6$, 1.27 for $Cs_2InBiBr_6$ and 0.65 eV for Cs_2InBiI_6, correspondingly [12].

Yasir Saeed *et al.* examined the physical features of Cs_2XGaBr_6 (X= Li, Na) discovering E_g of 0.45 and 0.731 eV for $Cs_2NaGaBr_6$ and $Cs_2LiGaBr_6$, respectively [13]. Mahmood *et al.* examined the Cs_2GeCl/Br_6 double perovskites for utilization in solar cell and thermoelectric devices, and thus, predicted ZT values of 0.80 for Cs_2GeCl_6 and 0.82 for Cs_2GeBr_6 at ambient temperature, respectively [14].

Comprehensive knowledge of the electronic characteristics of HDPs is the vital factor for the knowledge of macroscopic phenomena such as high conductivity and inter-band transitions from valance band (VB) to conduction band (CB) [15] [16]. However, a computational investigation of the electronic BS and DOS has not been formerly carried out for Sc as well as Y-based HDPs. The goal of the current study is to apply a comprehensive theoretical evaluation of TE, structural, and optoelectronic features of Cs_2XAgCl_6 (X= Sc, Y) by using the DFT.

2. Computational details

The full potential linearized augmented plane wave (FP-LAPW) approach is utilized in this computational investigation under DFT employed in the WIEN2k code. Physical features of Cs_2XAgCl_6 (X= Sc, Y) are calculated by employing PBE+GGA exchange-correlation functional with the TB-mBJ potential [17] [18]. In FP-LAPW method, the three variables i.e., wave function, charge density, and potential are separated into two categories. Wave function and potential are extended within the spheres in the spherical harmonics, while, the plan waves, outside of the sphere as represented in the given equation:

$$V(r) = \begin{cases} \sum_{LM} V_{LM}(r) Y_{LM}(\hat{r}) & \text{inside sphere} \\ \sum_{K} V_{K} e^{fK.r} & \text{outside sphere} \end{cases} \qquad (1)$$

The interstitial and non-overlapping atomic muffin tin spherical portions constitute the unit cell. Expansion of wave function is done in plane wave by setting $R_{MT} \times K_{max} = 7$ in interstitial region while it is expanded into spherical harmonics by setting l_{max} to 10 in muffin tin section. R_{MT} is muffin tin radii of atomic spheres located at the nuclei site and K_{max} represents to highest K-vector value. The R_{MT} value of 2.5 a.u is taken for Cs, Y, Sc, and Ag however for Cl atom it is 2.3 a. u. A mesh of $10 \times 10 \times 10$ k-points is considered to perform the calculation of compounds in the first Brillouin zone. For self-consistency, the computation is conducted in iterative manner until the discrepancy between successive iterations became smaller than 0.01 mRy. TE characteristics are calculated by utilizing the BoltzTraP code. Electronic configuration of Cesium (Cs), Silver (Ag), Scandium (Sc), Yttrium (Y) and Chlorine (Cl) are [Xe] $6s^1$, [Kr] $4d^{10} 5s^1$, [Ar] $3d^1 4s^2$, [Kr] $4d^1 5s^2$ and [Ne] $3s^2 3p^5$, correspondingly.

3. Results and discussions

3.1. Structural characteristics

Cs_2XAgCl_6 (X= Sc, Y) crystallize cubically with the space group Fm3m (#225). For the calculations of ground-state characteristics optimization (energy vs volume) curve is fitted in Birch-Murnaghan equation [19] and computed parameters are enlisted in Table 1 for nonmagnetic (NM) phase of both compounds while the equation is provided below:

$$E(V) = E_0 + \frac{9B_0V_0}{16}\left[\left\{\left(\frac{V_0}{V}\right)^{\frac{2}{3}} - 1\right\}^2 2\left\{3 - 2\left(\frac{V_0}{V}\right)^{\frac{2}{3}}\right\} + \left\{\left(\frac{V_0}{V}\right)^{\frac{2}{3}} - 1\right\}^3 B'_0\right] \quad (2)$$

Here, E(V) signifies internal energy, V_0 for equilibrium, and V for distorted volumes. B_0 and B'_0 indicate bulk modulus and its pressure derivative where bulk modulus can be obtained by utilizing the subsequent equation:

$$B_o = -V\frac{\partial P}{\partial V} = V\frac{\partial^2 E}{\partial V^2} \quad (3)$$

Table 1. The pressure derivative (B_0'), lattice constant, bulk modulus, and Formation energy ΔE (Ry) Cs_2XAgCl_6 (X= Sc, Y).

Parameters	$Cs_2ScAgCl_6$	Cs_2YAgCl_6
Lattice constant (Å)	19.6535	20.8162
Bulk modulus (GPa)	34.5763	26.6549
Pressure derivative (Bp)	4.3290	4.7573
Volume (a.u.)^3	1897.7320	2254.8056
Formation energy E_0 (Ry)	-48835.974	-78773.302677
Tolerance factor (τ)	0.99	1.00

The formula $E = E_{NM} - E_{FM}$ is employed to calculate the difference in energy between the NM and FM levels for the two materials. The analysis showed that the NM state released greater amount of energy, suggesting that both HDPs are more stable in NM states than FM phases. $Cs_2ScAgCl_6$ and Cs_2YAgCl_6 crystal structures and optimized energy vs volume curves are shown in Fig. 1. In the unit cells of Cs_2XAgCl_6 (X= Sc, Y), the Cs atom lies at 8c (1/4, 1/4, 1/4), X on 4a (0, 0, 0), Ag is positioned at 4b (0.5,0.5, 0.5), and Cl at 24e (x, 0, 0) Wyckoff (WP) positions.

To check the stability of materials, enthalpy of formation (ΔH_f) is calculated by the relation [20]:

$$\Delta H_f = E_{total} - aE_{Cs} - bE_{(X= Sc,Y)} - cE_{Ag} - dE_{Cl} \quad (4)$$

where a, b, c, d represent atom numbers for Cs, X, Ag, Cl while E_{total} is the total formation energy of Cs_2XAgCl_6 compound [21,22]. The results of formation energy are negative which authenticate stable thermodynamic nature for the studied HDPs. Structural stability of compounds in cubic phase is verified by determining τ which can be defined as:

$$\tau = \frac{0.707(R_{Cs} + R_{Cl})}{(R_{Avg} + R_{Cl})} \quad (5)$$

Here, R_{Cl} and R_{Cs} are ionic radii of Cl and Cs while R_{Avg} is the average ionic radius of Ag and X (X= Sc, Y) atoms, correspondingly. The value between 0.9 and 1.0 is regarded as stable, although the stability of perovskite materials is thought to be best in the range of 0.80-0.90 [23].

The τ value for $Cs_2ScAgCl_6$ is calculated as 0.97 and 0.93 for Cs_2YAgCl_6 which confirms the stable structure for both materials.

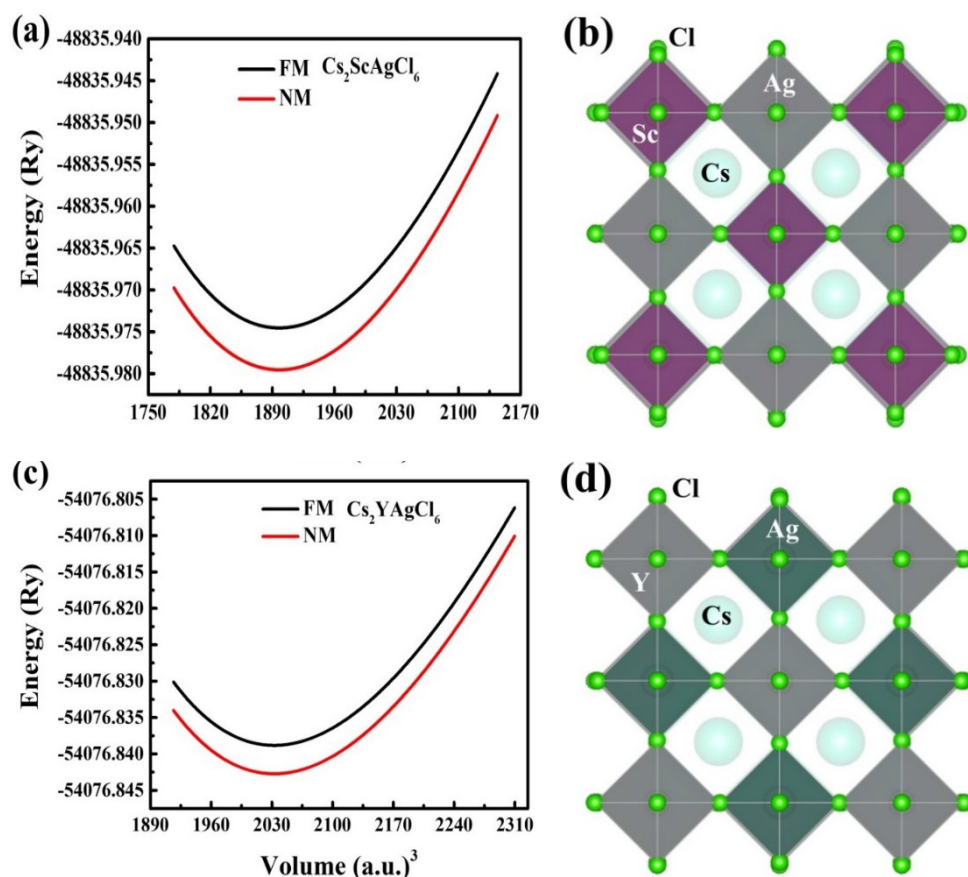*Fig. 1. (a, c) Optimization curve, and (b, d) Crystal Structure of $Cs_2ScAgCl_6$, and Cs_2YAgCl_6, correspondingly*

3.2. Electronic properties

In this part, the DOS and BS of Cs_2XAgCl_6 (X= Sc, Y) are explained. BS provides details regarding the conductivity of substances and is connected to the structure of the crystal [24]. BS for Cs_2XAgCl_6 (X= Sc, Y) are calculated by using mBJ potential. It is well known that the results calculated by mBJ potential for solids are closer to those achieved by experiments when compared to the GGA approximation.

Table 2. Computed values of Band gaps.

Compounds	Bandgap (eV)
$Cs_2ScAgCl_6$	3.78
Cs_2YAgCl_6	4.86

$Cs_2AgScCl_6$ and Cs_2YAgCl_6 exhibit E_g of 3.78 and 4.86 eV, respectively (see Fig. 2). Cs_2AgYCl_6 has a PBE0 bandgap of 6.08 eV [25], which is comparable to this reported E_g to some extent. The value of E_g decreases while moving from Yttrium (Y) to Scandium (Sc). This decrease is due to an increase in the amount of energy in the CB as the number of electrons rises, leading to an increase in repulsion between them. The reported values of E_g are suitable for the

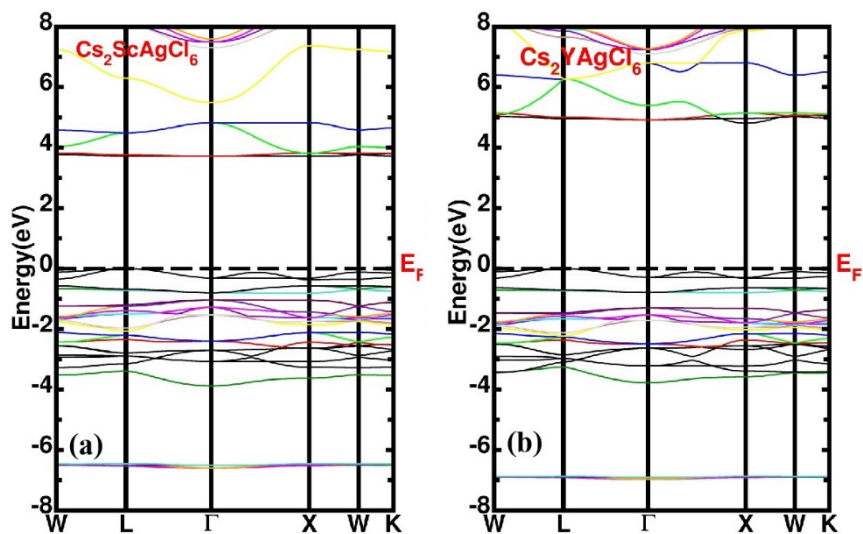production of renewable energy. The computed values of E_g for $Cs_2ScAgCl_6$ and Cs_2YAgCl_6 are displayed in Table 2.

Fig. 2. BS of (a) $Cs_2ScAgCl_6$ and (b) Cs_2YAgCl_6.

To comprehend the ramifications of bonding properties, the total and partial DOS of Cs_2XAgCl_6 (X= Sc, Y) have been determined using mBJ potential (see Fig. 3 (a & b)) within -8 to +8 eV energy spectrum.

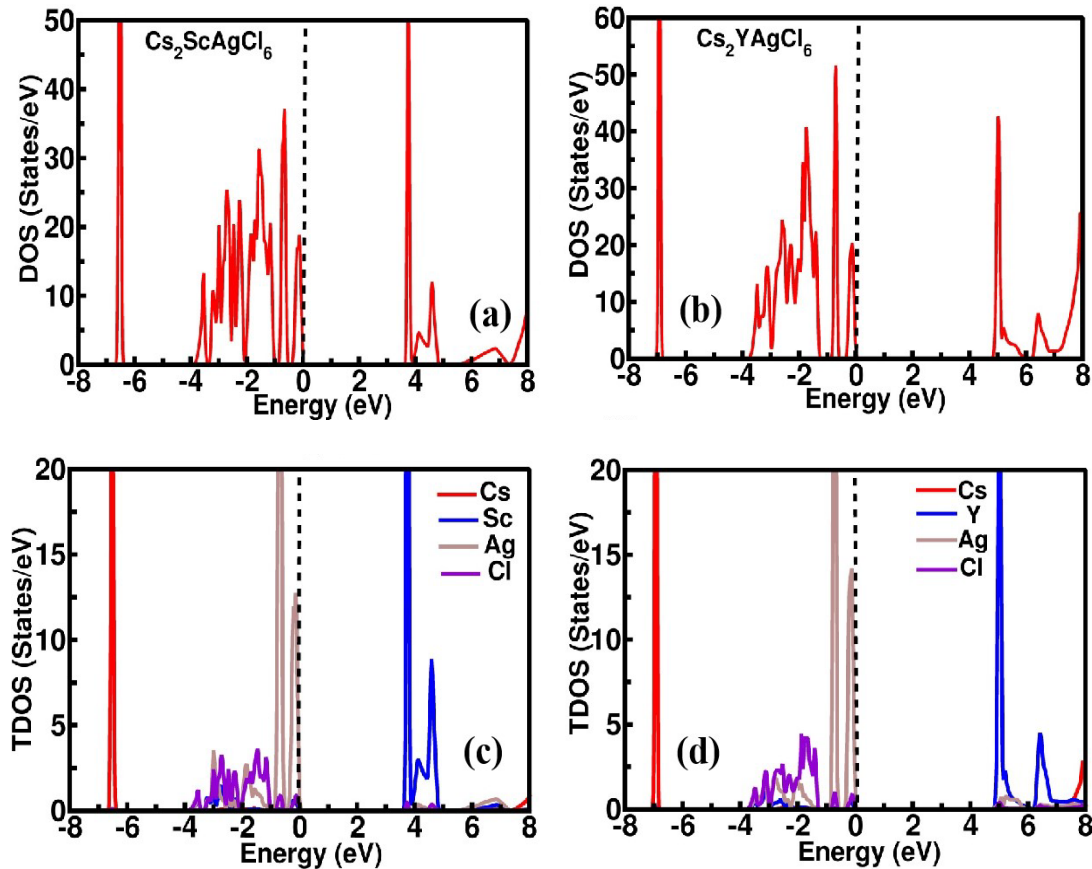*Fig. 3. DOS of (a) $Cs_2ScAgCl_6$, (b) DOS of Cs_2YAgCl_6, (c)TDOS of $Cs_2ScAgCl_6$, (d) TDOS of Cs_2YAgCl_6.*

Typically, DOS diagrams demonstrated how states contribute to the creation of bands [26]. More precisely, DOS spectra give suggestions about the transport characteristics of the compound. The entire TDOS calculations of both compounds displayed that the upper VB is mainly contributed by the Ag atom with a little bit contribution of halide atom (Cl). While in the formation of CB, Sc- atom played an important role in $Cs_2ScAgCl_6$ and Y-atom in Cs_2YAgCl_6 as depicted in Fig. 3(c&d). In PDOS d_{eg} states of Cs, Ag Sc, and Y show large role in VB from -3.98 to -1.0 eV for both $Cs_2ScAgCl_6$ and Cs_2YAgCl_6 while d-t_{2g} states of these atoms played main role in the CB as shown Fig. 4 and Fig. 5.

From DOS spectra, d_{eg} and d-t_{2g} showed more contribution in the semiconducting behavior for both compounds and both materials can be considered as the best applicants for their transport characteristics provided with greater dispersion in BS.
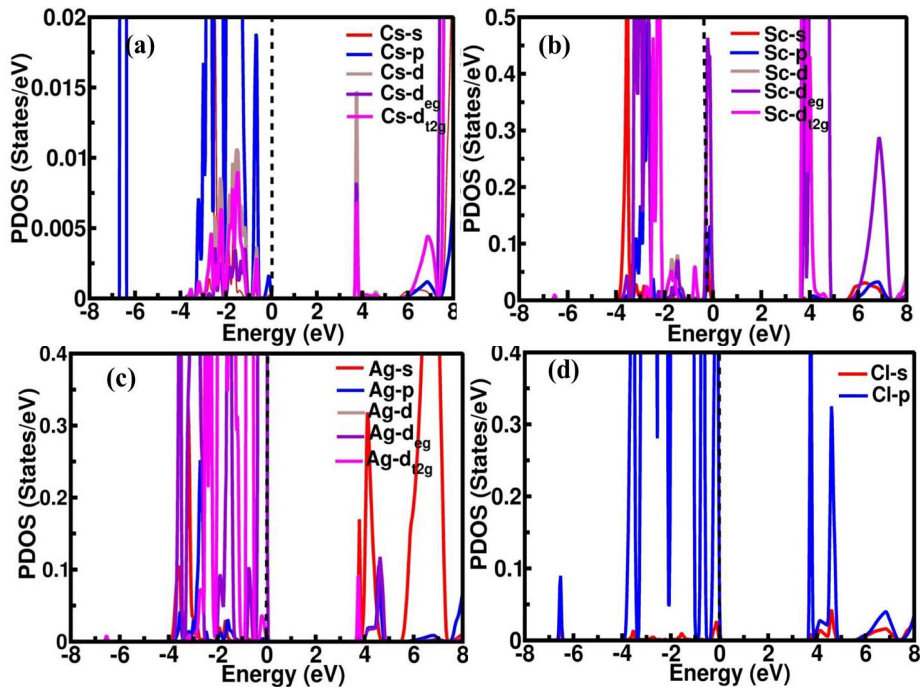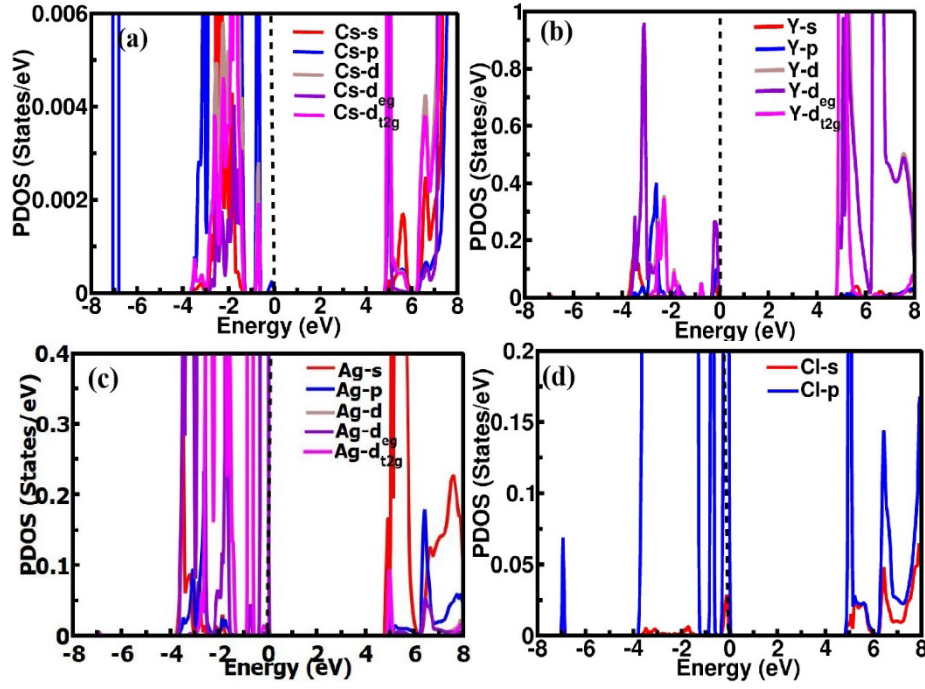

Fig. 4. PDOS of $Cs_2ScAgCl_6$.

Fig. 5. PDOS of Cs₂YAgCl₆.

3.2. Optical characteristics

It is necessary to comprehend the optical features of the materials for their usage in optoelectronic devices [27,28]. The frequency dependent ε(ω) provides an explanation that how an incoming photon interacts with an atom, which is comprised of two sections $\varepsilon_1(\omega)$ (real) and $\varepsilon_2(\omega)$ (imaginary) [29] as:

$$\varepsilon(\omega) = \varepsilon_1(\omega) + i\varepsilon_2(\omega) \tag{6}$$

$\varepsilon_1(\omega)$ describes light polarization and scattering power of material [30] [31] and is formulated as:

$$\varepsilon_1(\omega) = 1 + \frac{2}{\pi}p\int_0^\theta \frac{\omega'\varepsilon_2(\omega')}{\omega'^2 - \omega^2}d\omega' \tag{7}$$

where p denotes the principal value of integral. Maximum value of $\varepsilon_1(\omega)$ is noted to be 4.9 for Cs₂ScAgCl₆ at 4.2 eV while for Cs₂YAgCl₆ is 6.2 at 5.2 eV. Cs₂YAgCl₆ shows more scattering as compared to Cs₂ScAgCl₆ (see Fig. 6(a)). The inverse relation of $\varepsilon_1(0)$ and E_g is depicted by Penn's law as: $\varepsilon_1(0) \approx 1 + (\hbar\omega_p/E_g)^2$, while the relationship between $\varepsilon_2(\omega)$ and incident light is direct [32]:

$$\varepsilon_2(\omega) = \frac{e^2\hbar}{\pi m^2\omega^2}\sum_{VC}\int |n,n'(k,q)|^2\,\delta[\omega_{n,n'}(k) - \omega]d^3k \tag{8}$$
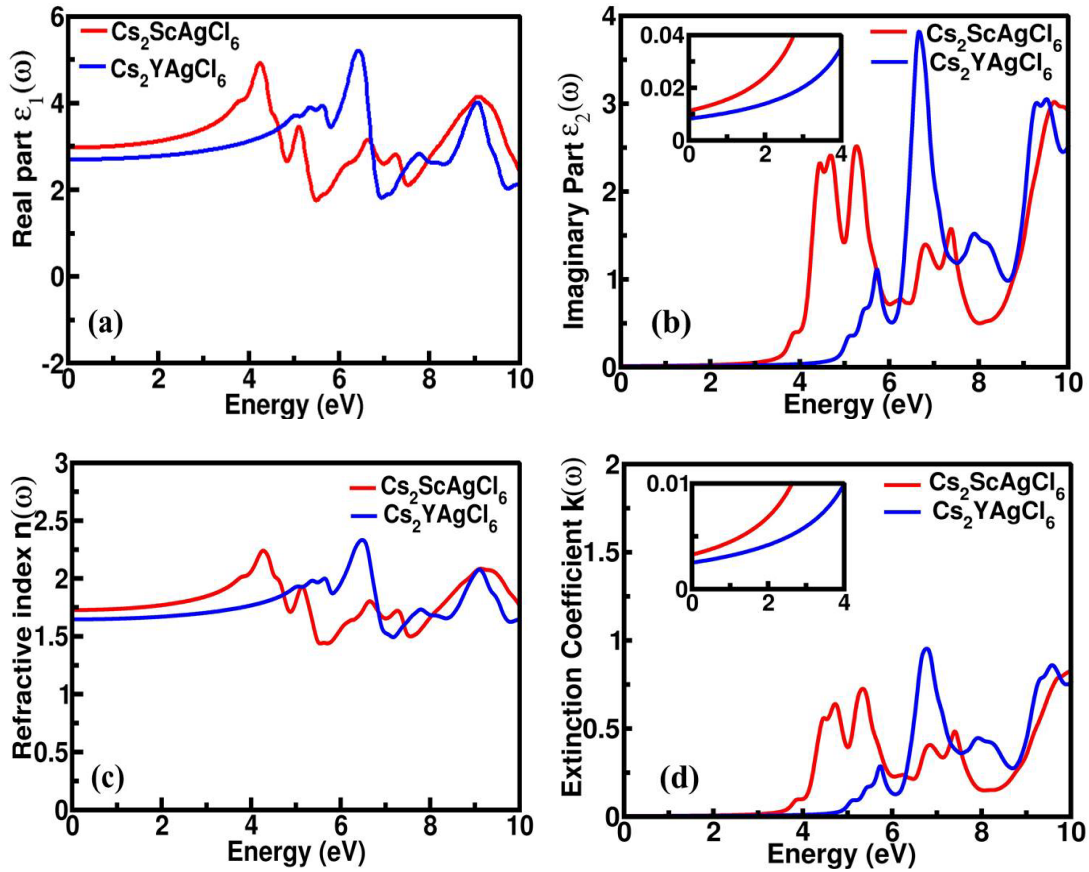
Fig. 6. (a) $\varepsilon_1 (\omega)$, (b) $\varepsilon_2 (\omega)$, (c) $n (\omega)$ and (d) $k (\omega)$ of Cs_2XAgCl_6 (X= Sc, Y).

Initially, there is no change seen in $\varepsilon_2(\omega)$ until the energy reached 3 eV. The first peak for $\varepsilon_2(\omega)$ is noticed at 4.4 eV for $Cs_2ScAgCl_6$ (presented in Fig. 6(b)) while peak for Cs_2YAgCl_6 is at 6.6 eV, which indicate that Cs_2XAgCl_6 (X= Sc, Y) are suitable for optoelectronic applications.

$n(\omega)$ represents the penetration ability of EM waves through materials. To check the effectiveness of materials for solar cells and detectors refractive index is studied (see Fig. 6 (c)). It is dimensionless and has inverse relation with bandgap energy. $n(\omega)$ is determined by the given relation [33].

$$n(\omega) = \sqrt{\frac{[\varepsilon_1^2(\omega)+\varepsilon_2^2(\omega)]^{\frac{1}{2}}+ \varepsilon_1(\omega)}{2}} \qquad (9)$$

It is seen that the highest peak of about 2.2 for $Cs_2ScAgCl_6$ is at 4.2 eV, but for Cs_2YAgCl_6 maximum value of 2.33 is observed at 6.4 eV. Several other peaks were observed due to the discrete energy bands. For both compounds, all the spectral peaks are located within the ultraviolet (UV) range. The variation observed in $n(\omega)$ is aligned with the trends observed in $\varepsilon_1(\omega)$. $k(\omega)$ represents absorption ability of the material and can be obtained by the equation:

$$k(\omega) = \sqrt{\frac{[\varepsilon_1^2(\omega)+\varepsilon_2^2(\omega)]^{\frac{1}{2}}- \varepsilon_1(\omega)}{2}} \qquad (10)$$

$k(\omega)$ started from 3.7 eV for $Cs_2ScAgCl_6$ and from 4.7 eV for Cs_2YAgCl_6 due to absorption of incident photons [34]. Initially, there is no change noticed in the $k(\omega)$ spectrum. When energies reached at 5.32/6.7 eV, the maximum peaks of 0.72/0.97 (see Fig. 6(d)) are observed for $Cs_2ScAgCl_6$/Cs_2YAgCl_6, correspondingly.

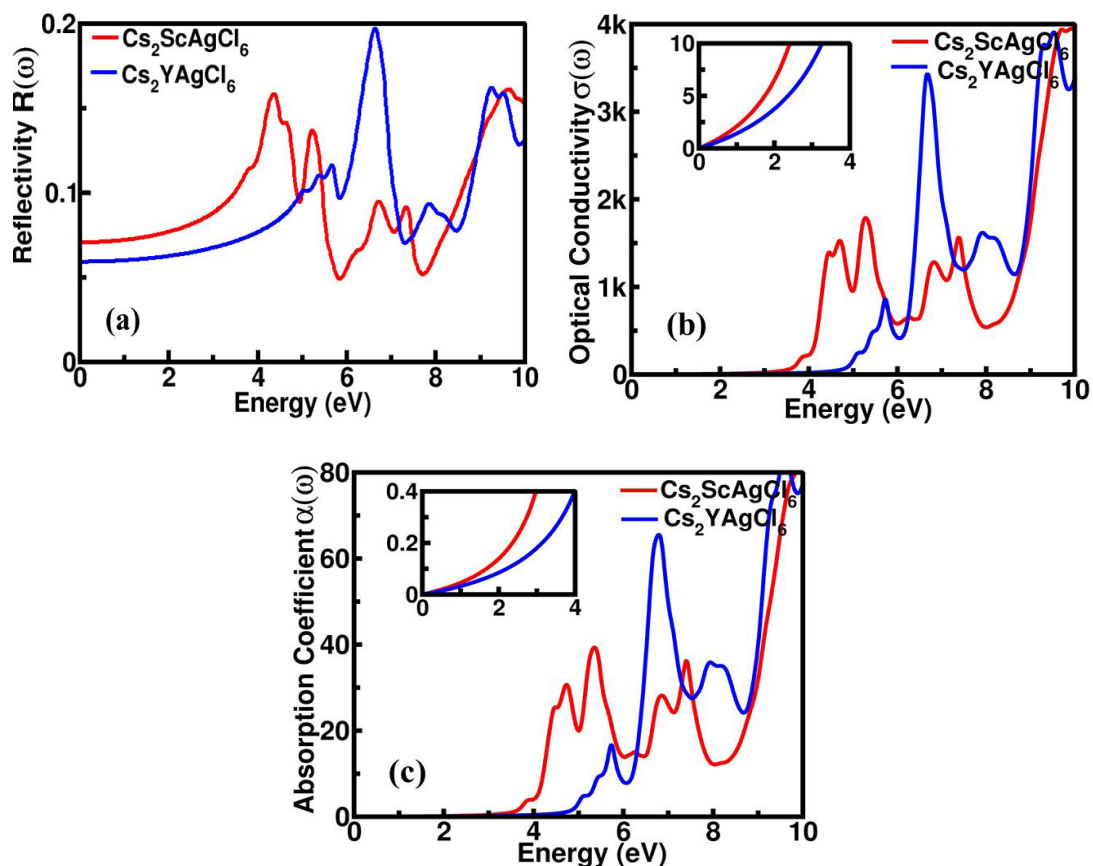*Fig. 7. (a) R (ω), (b) σ(ω) and (c)α (ω) of K₂NaXBr₆ (X= Sc, Y).*

Another important optical factor is reflectivity R(ω) which is measured by the given relation:

$$R(\omega) = \frac{(n-1)^2+k^2}{(n+1)^2+k^2} = \left|\frac{n'-1}{n'+1}\right| \tag{11}$$

To examine how HDPs react to an incoming beam, R(ω) is analysed. R(ω) is found to follow same trend as ε₁(ω) of the dielectric constant. The highest value of about 0.15 (at 4.3 eV) and 0.19 (at 6.6 eV) appeared for Cs₂ScAgCl₆ and Cs₂YAgCl₆, correspondingly (see Table 3). After this, the R(ω) started to decrease with fluctuations see Fig. 7(a).

Optical conductivity σ(ω) interprets electronic conductivity under photon field. For both materials, σ(ω) initiated from the band gap edge. The UV zone has the highest value of σ(ω), as there is a significant rate of absorption in this area (see Fig.7(b)). The α(ω) is another parameter for investigation of optoelectronic applications. α(ω) is directly related to both k(ω) and ε₂(ω). The relation between the extinction and absorption coefficients is expressed as:

$$\alpha(\omega) = \frac{4\pi k(\omega)}{\lambda} \tag{12}$$

For both halides, each peak is in the UV region (see Fig. 7(c)), which indicates that both materials can be competently used in optoelectronic applications.

Table 3. The calculated values of Optical parameters for Cs_2XAgCl_6 (X= Sc, Y).

Optical Parameters	$Cs_2ScAgCl_6$	Cs_2AgYCl_6
$\varepsilon_1(0)$	4.9	6.2
$n(0)$	2.2	2.33
$R(0)$	0.15	0.19

3.3. Thermoelectric (TE) properties

Heat can be converted into electrical energy by using TE materials [35]. Therefore, to overwhelm the environmental thermal pollution, it is necessary to study the thermoelectric characteristics of Cs_2XAgCl_6 (X= Sc, Y) in search of their suitability as TE materials. The bandgap is important for obtaining the transport characteristics of TE compounds [36]. TE parameters like figure of merit (ZT), thermal conductivity (k/τ), power factor (PF), seebeck coefficient (S), and electrical conductivity (σ/τ) are figured out for $Cs_2ScAgCl_6$ and Cs_2YAgCl_6 by using the BoltzTraP code with a constant scattering time ($\tau = 10^{-14}$ s).

With an increase in temperature, σ/τ rises for Cs_2XAgCl_6 (X= Sc, Y) compounds which confirmed the semiconductor nature of both materials (see Fig. 8(a)). Narrow-band semiconductors exhibit superior TE material characteristics owing to their high charge carrier mobility compared to conventional semiconductors [37]. Highest computed values of σ/τ for both compounds are given in Table 4. The k/τ of $Cs_2ScAgCl_6$ and Cs_2YAgCl_6 are shown in Fig. 8(b).
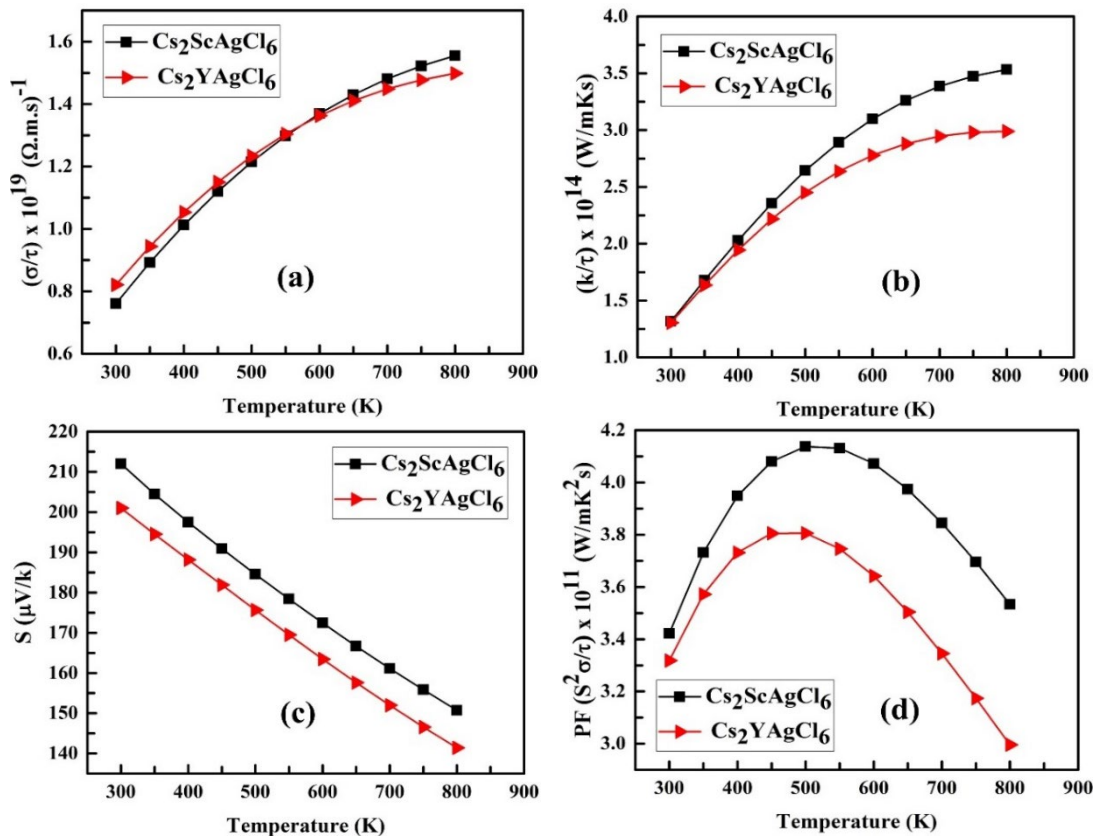
Fig. 8. The obtained values of (a) σ/τ (b) S, (c) PF (d) k/τ.

Values of k/τ depend upon the contribution of phonons as well as electrons for semiconductors. In the current study, only the electronic contribution is taken into account while the phonon contribution is neglected as it has no significant effect at high temperature. The k/τ

rises with rising temperature following same trend as σ/τ. The k/τ of $Cs_2ScAgCl_6$ is higher than that of Cs_2YAgCl_6 because of the greater number of electrons available in $Cs_2ScAgCl_6$ than Cs_2YAgCl_6. The computed thermal conductivity of both compounds at 300 K is 1.3169 W/mKs, with the greatest values of 3.5337 and 2.9889 W/mKs for $Cs_2ScAgCl_6$ and Cs_2YAgCl_6, respectively, at 800 K. The relationship between σ/τ and k/τ is described by the Wiedemann-Franz principle, which is stated by the equation LT= k/σ. The order $x10^5$ values derived from the k/σ ratio indicated that such substances might be employed in TE devices [38].
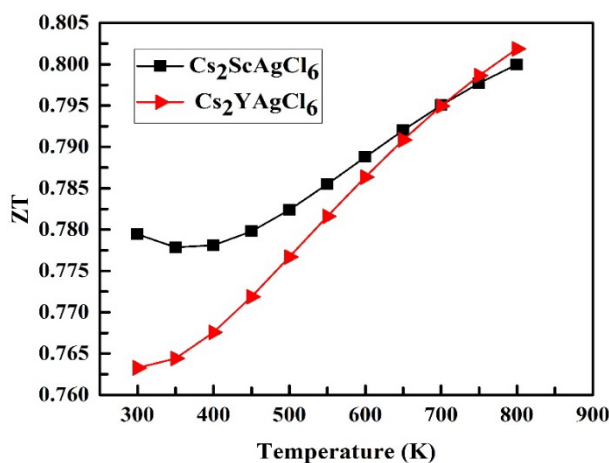

Fig. 9. ZT versus temperature range 300-800 K of Cs_2XAgCl_6 (X= Sc, Y).

The voltage to temperature change ratio is known as the Seebeck coefficient (S). It is revealed that S has an inverse relation with σ/τ and k/τ [39] [40]. A positive S value signifies the compound as p-type material, characterized by a predominance of holes. Conversely, a negative S value indicates the n-type nature of the materials, where electrons dominate [41]. Current evaluation has shown positive values of S which confirmed the dominance of holes and thus revealed p-type nature of both HDPs. Initially, S has highest values of 212 and 201.02 μV/k for $Cs_2ScAgCl_6$ and Cs_2YAgCl_6, correspondingly, as depicted in Fig. 8(c) and is determined by given formula:

$$S = \frac{\Delta V}{\Delta T} \tag{13}$$

With the rise of temperature, S started to decrease until it reaches to its least value due to the thermally excited minority carriers. One of the main factors to explore the TE performance of any material is the power factor (PF). Materials having higher PF values are thought to be more thermoelectrically efficient as PF has direct link with ZT [20]. The initial trend of PF is linear and its spectrum shows its peak values of 3.78×10^{11} and 4.1×10^{11} W/K^{2}s at 450 and 500 K temperature (see Fig 8(d)) for Cs_2YAgCl_6 and $Cs_2ScAgCl_6$, correspondingly.

ZT is utilized to assess the effectiveness of the materials [42][43]. ZT has no dimensions, and the following expression represents the collective influence of σ, S, k, and T on the system as ZT:

$$ZT = \frac{S^2 \sigma T}{k} \tag{14}$$

The maximum magnitude of ZT is 0.80 for Cs_2YAgCl_6 and 0.79 for $Cs_2ScAgCl_6$ as shown in Fig. 9 (at 800 K). Therefore, both compounds are recommended as efficient materials for thermoelectric applications.

Table 4. At 800 K temperature calculated values of thermoelectric coefficients for Cs_2XAgCl_6 (X= Sc, Y).

Materials	$\sigma/\tau \times 10^{19}$ $(\Omega.m.s)^{-1}$	Seebeck coefficient $(\frac{\mu V}{k})$	k/τ $\times 10^{14}$(W/mKs)	PF $\times 10^{11}$ (W/mK^{2}s)	ZT
$Cs_2ScAgCl_6$	1.555	150.73	3.533	3.5336	0.7999
Cs_2YAgCl_6	1.498	141.39	2.988	2.995	0.8018

4. Conclusion

DFT computations were conducted in current study to investigate the optoelectronic, structural, and TE features of Cs_2XAgCl_6 (X= Sc, Y) by the FP-LAPW method. The structural analysis confirmed that both compounds possess a cubic crystal structure, exhibiting the Fm3m space group. The confirmation of the thermodynamically stable structure of both compounds is reinforced by the negative values observed from the calculations of formation energies The results obtained from BS demonstrated the semiconductor nature of both materials with E_g of 3.78/4.86 eV for $Cs_2ScAgCl_6$/Cs_2YAgCl_6, correspondingly. TDOS and PDOS revealed that both Sc and Y played a substantial role in CB while Cl in VB caused semiconducting features. The analysis of the optical features revealed a large $\alpha(\omega)$ and a small $R(\omega)$ value which made both compounds suitable candidates for optoelectronic applications. Moreover, ZT is calculated as 0.80 for Cs_2YAgCl_6 and 0.79 for $Cs_2ScAgCl_6$ at 800 K, which suggested both materials to have possible applications in TE appliances.

Acknowledgement

References

[1] K.A. Parrey, S.A. Khandy, I. Islam, A. Laref, D.C. Gupta, A. Niazi, A. Aziz, S.G. Ansari, R. Khenata, S. Rubab, Journal of Electronic Materials. 47, 3615–3621 (2018); https://doi.org/10.1007/s11664-018-6207-8.
[2] S. Mubashir, M.K. Butt, M. Yaseen, J. Iqbal, M. Iqbal, A. Murtaza, A. Laref, Optik. 239, 166694 (2021); https://doi.org/10.1016/j.ijleo.2021.166694.
[3] S.A. Mir, D.C. Gupta, RSC Adv. 10, 26277–26287 (2020); https://doi.org/10.1039/d0ra02817g.
[4] B. Kou, W. Zhang, C. Ji, Z. Wu, S. Zhang, X. Liu, J. Luo, Chemical Communications. 55, 14174–14177 (2019); https://doi.org/10.1039/c9cc05365d.
[5] E.T. McClure, M.R. Ball, W. Windl, P.M. Woodward, Chemistry of Materials. 28, 1348–1354 (2016); https://doi.org/10.1021/acs.chemmater.5b04231.
[6] E. Haque, M.A. Hossain, condensed matter. (2018); http://arxiv.org/abs/1802.08136.
[7] Y.J. Li, T. Wu, L. Sun, R.X. Yang, L. Jiang, P.F. Cheng, Q.Q. Hao, T.J. Wang, R.F. Lu, W.Q. Deng, RSC Adv. 7, 35175–35180 (2017); https://doi.org/10.1039/c7ra06130g.
[8] A.H. Slavney, T. Hu, A.M. Lindenberg, H.I. Karunadasa, J Am Chem Soc. 138, 2138–2141 (2016); https://doi.org/10.1021/jacs.5b13294.
[9] M.R. Filip, S. Hillman, A.A. Haghighirad, H.J. Snaith, F. Giustino, Journal of Physical Chemistry Letters. 7, 2579–2585 (2016); https://doi.org/10.1021/acs.jpclett.6b01041.
[10] A. Soni, K.C. Bhamu, J. Sahariya, J Alloys Compd. 817 152758 (2020); https://doi.org/10.1016/j.jallcom.2019.152758.

[11] N.A. Noor, M.W. Iqbal, T. Zelai, A. Mahmood, H.M. Shaikh, S.M. Ramay, W. Al-Masry, Journal of Materials Research and Technology. 13, 2491–2500 (2021); https://doi.org/10.1016/j.jmrt.2021.05.080.

[12] A. Fatima, U. Hamid, H. M., Materials Science and Engineering: B. 274 115456 (2021); https://doi.org/https://doi.org/10.1016/j.mseb.2021.115456.

[13] Y. Saeed, B. Amin, H. Khalil, F. Rehman, H. Ali, M.I. Khan, A. Mahmood, M. Shafiq, RSC Adv. 10, 17444–17451 (2020); https://doi.org/10.1039/d0ra01764g.

[14] Q. Mahmood, T. Ghrib, A. Rached, A. Laref, M.A. Kamran, Mater Sci Semicond Process. 112, 105009 (2020); https://doi.org/10.1016/j.mssp.2020.105009.

[15] M. Huma, M. Rashid, Q. Mahmood, E. Algrafy, N.A. Kattan, A. Laref, A.S. Bhatti, Mater Sci Semicond Process. 121, 1–7 (2021); https://doi.org/10.1016/j.mssp.2020.105313.

[16] A.H. Slavney, L. Leppert, D. Bartesaghi, A. Gold-Parker, M.F. Toney, T.J. Savenije, J.B. Neaton, H.I. Karunadasa, Journal of the American Chemical Society. 139, 5015-5018 (2017); https://doi.org/10.1021/jacs.7b01629.

[17] M.I.H. Ansari, A. Qurashi, M.K. Nazeeruddin, Journal of Photochemistry and Photobiology C: Photochemistry Reviews. 35, 1–24 (2018); https://doi.org/10.1016/j.jphotochemrev.2017.11.002.

[18] A. Mokhtari, H. Akbarzadeh, Physica B Condens Matter. 324, 305–311 (2002); https://doi.org/10.1016/S0921-4526(02)01416-3.

[19] B. Hammer, L.B. Hansen, J.K. Nørskov, Phys Rev B Condens Matter Mater Phys. 59, 7413–7421 (1999); https://doi.org/10.1103/PhysRevB.59.7413.

[20] Nasarullah, M. Yaseen, S.A. Aldaghfag, M. Zahid, Misbah, Mater Sci Semicond Process. 147, 106760 (2022); https://doi.org/10.1016/j.mssp.2022.106760.

[21] Hafsa, M. Ishfaq, S.A. Aldaghfag, M. Yaseen, Nasarullah, U. Younis, R. Neffati, J Solid State Chem. 322, 123999 (2023); https://doi.org/10.1016/j.jssc.2023.123999.

[22] A. Gilani, Nasarullah, S.A. Aldaghfag, M. Yaseen, Journal of Physics and Chemistry of Solids. 175, 111208 (2023); https://doi.org/10.1016/j.jpcs.2022.111208.

[23] Nasarullah, M.Z. Choudary, S.A. Aldaghfag, Misbah, M. Yaseen, M. Nazar, R. Neffati, Phys Scr. 97, 105705 (2022); https://doi.org/10.1088/1402-4896/ac8c6e.

[24] S.A. Dar, R. Sharma, V. Srivastava, U.K. Sakalle, RSC Adv. 9, 9522–9532 (2019); https://doi.org/10.1039/c9ra00313d.

[25] M.H. Du, K. Biswas, J Lumin. 143, 710–714 (2013); https://doi.org/10.1016/j.jlumin.2013.05.033.

[26] Nasarullah, A. Younas, Z.M. Elqahtani, S.A. Aldaghfag, M. Yaseen, M. Zahid, H.H. Somaily, Phys Status Solidi B Basic Res. 259, 2200189 (2022); https://doi.org/10.1002/pssb.202200189.

[27] M. Arshad, M. Yaseen, S. A. Aldaghfag, S. Saleem, M. Ishfaq, M. Nazar, E. Yousef, H. H. Hegazy, Chalcogenide Lett 19(8), 553-563 (2022); https://doi.org/10.15251/CL.2022.198.553.

[28] M. Nazar, Nasarullah, S.A. Aldaghfag, M. Yaseen, M. Ishfaq, R.A. Khera, S. Noreen, M.H. Abdellattif, Journal of Physics and Chemistry of Solids. 166, 110719 (2022); https://doi.org/10.1016/j.jpcs.2022.110719.

[29] S. Munir, M.K. Butt, S.A. Aldaghfag, Misbah, M. Yaseen, Nasarullah, M. Nazar, H.H. Somaily, Physica B Condens Matter. 645, 414252 (2022); https://doi.org/10.1016/j.physb.2022.414252.

[30] S.A. Mir, D.C. Gupta, J Alloys Compd. 854, 156000 (2021); https://doi.org/10.1016/j.jallcom.2020.156000.

[31] T. Ahmed, A. Chen, D.A. Yarotski, S.A. Trugman, Q. Jia, J.X. Zhu, APL Mater. 5 (2017). https://doi.org/10.1063/1.4964676.

[32] M. Nazar, Nasarullah, S.A. Aldaghfag, M. Yaseen, M. Waqas, M.K. Butt, I. Boukhris, Phys Status Solidi B Basic Res. 260, 2300003 (2023); https://doi.org/10.1002/pssb.202300003.

[33] Q. Mahmood, M. Hassan, M.A. Faridi, Chinese Physics B. 26, 027503 (2017); https://doi.org/10.1088/1674-1056/26/2/027503.

[34] I. Khan, Shahab, I.U. Haq, A. Ali, Z. Ali, I. Ahmad, J Electron Mater. 50, 456–466 (2021); https://doi.org/10.1007/s11664-020-08603-y.

[35] I. Khan, A.U. Rahman, I.U. Haq, I. Ahmad, Z. Ali, Computational Condensed Matter. 21, 1–10 (2019); https://doi.org/10.1016/j.cocom.2019.e00427.

[36] G.K.H. Madsen, D.J. Singh, BoltzTraP. A code for calculating band-structure dependent quantities, Comput Phys Commun. 175, 67–71 (2006); https://doi.org/10.1016/j.cpc.2006.03.007.

[37] S. Haid, W. Benstaali, A. Abbad, B. Bouadjemi, S. Bentata, Z. Aziz, Mater Sci Eng B Solid State Mater Adv Technol. 245, 68–74 (2019); https://doi.org/10.1016/j.mseb.2019.05.013.

[38] S.A. Khandy, D.C. Gupta, RSC Adv. 6, 48009–48015 (2016); https://doi.org/10.1039/c6ra10468a.

[39] N. Arikan, G. DikiCi Yildiz, Y.G. Yildiz, A. İyigör, J Electron Mater. 49, 3052-3062 (2020); https://doi.org/10.1007/s11664-020-08029-6.

[40] S. Chettri, D.P. Rai, A. Shankar, R. Khenata, M.P. Ghimire, R.K. Thapa, S. Bin Omran, Int J Mod Phys B. 30, 1650078 (2016); https://doi.org/10.1142/S0217979216500788.

[41] S. Das, M. Debbarma, D. Ghosh, S. Chanda, B. Debnath, R. Bhattacharjee, S. Chattopadhyaya, Physica B Condens Matter. 626, 413554 (2022); https://doi.org/10.1016/j.physb.2021.413554.

[42] M. Yaseen, H. Ambreen, A. Sufyan, M.K. Butt, S. UrRehman, J. Iqbal, M. Misbah, S. Bibi, A. Murtaza, S.M. Ramay, Ferroelectrics. 557, 112–122 (2020); https://doi.org/10.1080/00150193.2020.1713356.

[43] T. Takeuchi, Mater Trans. 50, 2359–2365 (2009); https://doi.org/10.2320/matertrans.M2009143.